RESEARCH ARTICLE

Impact of volcanic aerosols on stratospheric ozone recovery

Vaishali Naik[1] [ID], Larry W. Horowitz[1] [ID], M. Daniel Schwarzkopf[1], and Meiyun Lin[1,2] [ID]

[1]NOAA Geophysical Fluid Dynamics Laboratory, Princeton, New Jersey, USA, [2]Program in Atmospheric and Oceanic Sciences, Princeton University, Princeton, New Jersey, USA

Abstract We use transient GFDL-CM3 chemistry-climate model simulations over the 2006–2100 period to show how the influence of volcanic aerosols on the extent and timing of ozone recovery varies with (a) future greenhouse gas scenarios (Representative Concentration Pathway (RCP)4.5 and RCP8.5) and (b) halogen loading. Current understanding is that elevated volcanic aerosols reduce ozone under high halogen loading but increase ozone under low halogen loading when the chemistry is more NO_x dominated. With extremely low aerosol loadings (designated here as "background"), global stratospheric ozone burden is simulated to return to 1980 levels around 2050 in the RCP8.5 scenario but remains below 1980 levels throughout the 21st century in the RCP4.5 scenario. In contrast, with elevated volcanic aerosols, ozone column recovers more quickly to 1980 levels, with recovery dates ranging from the mid-2040s in RCP8.5 to the mid-2050s to early 2070s in RCP4.5. The ozone response in both future emission scenarios increases with enhanced volcanic aerosols. By 2100, the 1980 baseline-adjusted global stratospheric ozone column is projected to be 20–40% greater in RCP8.5 and 110–200% greater in RCP4.5 with elevated volcanic aerosols compared to simulations with the extremely low background aerosols. The weaker ozone enhancement at 2100 in RCP8.5 than in RCP4.5 in response to elevated volcanic aerosols is due to a factor of 2.5 greater methane in RCP8.5 compared with RCP4.5. Our results demonstrate the substantial uncertainties in stratospheric ozone projections and expected recovery dates induced by volcanic aerosol perturbations that need to be considered in future model ozone projections.

Plain Language Summary Uncertainty in future levels of stratospheric aerosols from volcanic eruptions has been identified as a key uncertainty in predicting future stratospheric ozone abundance. We use transient GFDL-CM3 chemistry-climate model simulations over the 2006-2100 time period to show how the influence of volcanic aerosols on the extent and timing of ozone recovery varies with (a) future greenhouse gas scenarios (RCP4.5 and RCP8.5) and (b) halogen loading. We show that increased volcanic aerosol abundances would lead to earlier ozone recovery under the RCP4.5 and RCP8.5 scenarios. Projections of stratospheric ozone should consider volcanic aerosols.

1. Introduction

Stratospheric aerosols affect stratospheric ozone directly by affecting heterogeneous chemistry and photolysis rates, and indirectly by influencing stratospheric temperature and large-scale circulation patterns [*Stratospheric Processes and their Role in Climate [SPARC]*, 2006]. Recent measurements indicate that there has been a continuous increase in stratospheric aerosols over the last decade following a period (1998–2002) of "background" (nonvolcanic) aerosol levels. This increase has been attributed to a series of moderate tropical volcanic eruptions [*Vernier et al.*, 2011]. However, the impact of volcanic perturbations on the evolution of stratospheric ozone in the 21st century has not been considered in projections of long-term stratospheric ozone changes using chemistry-climate models [*Eyring et al.*, 2010a, 2013]. For example, volcanic aerosols were set to zero or to near-zero background in future climate projections conducted for the Coupled Model Intercomparison Project Phase 5 (CMIP5) [*Collins et al.*, 2013, Table 12.1]. Here we explore the evolution of stratospheric ozone over the 2006–2100 period in response to two future climate forcing scenarios under three different fixed levels of volcanic aerosol loading. We highlight the contrasting effects of volcanic aerosol amounts under high (e.g., present day) and low (e.g., future) halogen loading [e.g., *Austin et al.*, 2013], the differing responses to greenhouse gas abundances, and the resulting influence on the timing of ozone recovery.

Volcanic eruptions enhance the background stratospheric aerosol layer, first identified by *Junge et al.* [1961], by injecting large amounts of sulfur dioxide (SO_2) and ash. SO_2 oxidizes to sulfuric acid (H_2SO_4) which nucleates homogeneously or condenses on existing particles to form sulfate aerosols (H_2SO_4-H_2O). Volcanic sulfate

aerosols affect the Earth's radiative balance by increasing the scattering of incoming solar radiation and enhancing the infrared absorption depending on the particle size, thus cooling the Earth's surface and the troposphere, and warming the stratosphere [*McCormick et al.*, 1995]. The influence of volcanic aerosols on stratospheric ozone, particularly in the midlatitudes, via heterogeneous chemistry is also well known, as briefly discussed below.

Observational and modeling studies conducted after the Mount Pinatubo volcanic eruptions provided evidence of decreases in nitrogen oxides ($NO_x = NO + NO_2$) and increases in reactive halogen radicals via heterogeneous chemistry on sulfate aerosols [*Fahey et al.*, 1993; *Koike et al.*, 1994; *Wennberg et al.*, 1994]. As a result, the NO_x-catalyzed ozone loss is suppressed, particularly in the middle stratosphere where the NO_x cycle is efficient at destroying ozone [*Brasseur et al.*, 1999]. The reduction in NO_x also limits the formation of reservoir species, such as chlorine nitrate ($ClONO_2$) and bromine nitrate ($BrONO_2$), increasing the abundance of reactive halogen ($ClO_x = Cl + ClO$, $BrO_x = Br + BrO$), and to a lesser extent, hydrogen oxides ($HO_x = OH + HO_2$). Reactive halogen radicals are also enhanced due to heterogeneous activation on sulfate aerosols. Thus, the efficiency of ozone destruction by ClO_x, BrO_x, and HO_x cycles [*Wennberg et al.*, 1994; *Lary et al.*, 1996; *Solomon et al.*, 1996] is enhanced in the presence of volcanic sulfate aerosols (see *Solomon,* 1999 for a detailed review). The net impact of enhanced volcanic aerosols in the present atmosphere is to increase ozone in the middle stratosphere and decrease ozone in the lower stratosphere, resulting in a net decrease of ozone column. The overall effect on global ozone burden has been shown to depend on the halogen loading of the atmosphere [*Tie and Brasseur*, 1995; *Austin et al.*, 2013].

Multimodel projections of future ozone levels and the dates of ozone recovery to 1980 levels vary by latitude region and are dependent upon the assumed projections of well-mixed greenhouse gases (WMGGs), including carbon dioxide (CO_2), methane (CH_4), and nitrous oxide (N_2O), and ozone depleting substances (ODSs), as well as the resulting climate and stratospheric circulation changes [*Pawson et al.*, 2014]. The possibility of significant changes in stratospheric aerosol levels has been identified as a key uncertainty in predicting future ozone abundance by the World Meteorological Organization and United Nations Environment Programme Scientific Assessment of Ozone Depletion [*Bekki et al.*, 2011]. In this study, we perform transient 21st century simulations with the U.S. NOAA Geophysical Fluid Dynamics Laboratory (GFDL) fully interactive chemistry-climate model (GFDL-CM3) to assess ozone recovery in response to the Representative Concentration Pathway (RCP)4.5 and RCP8.5 climate forcing scenarios under three different assumptions of stratospheric aerosol loading.

2. Model Evaluation and Simulations

We employ the GFDL-CM3 chemistry-climate model [*Donner et al.*, 2011; *John et al.*, 2012; *Austin et al.*, 2013; *Westervelt et al.*, 2015; *Barnes et al.*, 2016] in this study. Transient historical (1860–2005) and future (2006–2100) simulations of CM3 were conducted in support of the Coupled Model Intercomparison Project (CMIP5) and informed the Intergovernmental Panel on Climate Change Assessment Report 5. CM3 uses a finite-volume dynamical core on a cubed-sphere horizontal grid composed of six faces, each with a horizontal domain of 48×48 grid cells, denoted as C48 horizontal resolution, where the size of the grid cells range from 163 km at the corners to 231 km near the face centers. CM3 includes 48 vertical hybrid sigma-pressure levels extending from the surface to 0.01 hPa (~80 km). Model output is regridded to a latitude-longitude grid with $2° \times 2.5°$ horizontal resolution for analysis. CM3 does not internally generate a quasi-biennial oscillation (QBO), the leading mode of variability in the tropical lower and middle stratosphere [*Baldwin et al.*, 2001]. The model simulates tropospheric and stratospheric gas phase and heterogeneous photochemical processes over the full model domain [*Austin et al.*, 2013; *Naik,* 2013]; the simulated three-dimensional ozone distribution influences radiation calculations. Stratospheric chemistry includes gas-phase reactions describing the HO_x, NO_x, ClO_x, and BrO_x catalytic cycles and heterogeneous reactions on solid nitric acid trihydrate (NAT) and water-ice polar stratospheric cloud (PSC) particles, and liquid binary and ternary sulfate particles [*Austin and Wilson*, 2010]. Global mean tropospheric volume mixing ratios of ozone depleting substances (ODSs) are specified as a function of time providing a parametrized source of reactive halogens to the stratosphere [*Austin et al.*, 2013]. These ODSs include chlorofluorocarbons (CFCs), hydrochlorofluorocarbons, halons, and an additional 4 pptv of bromine from very short-lived substances that have been shown to be important during periods of elevated stratospheric aerosols.
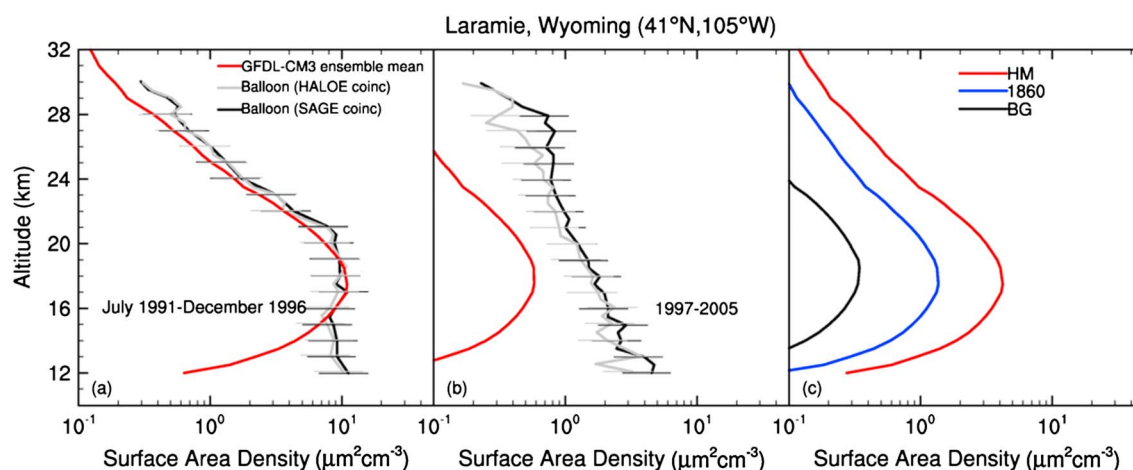
Figure 1. Vertical profiles of aerosol surface area density (SAD) implemented in the ensemble mean historical GFDL-CM3 simulation compared to in situ measurements at Laramie, Wyoming, from the University of Wyoming's balloon-borne optical particle counter (OPC) coincident with the SAGE II and HALOE satellite measurements [*Kovilakam and Deshler*, 2015] averaged for the (a) July 1991 to December 1996 (post-Pinatubo) and (b) 1997–2005 (low volcanic) time periods. The error bars show one standard deviation of the measurements. (c) Aerosol SAD vertical profiles at Laramie as implemented in the RCPX.X_BG, RCPX.X_1860, and RCPX.X_HM simulations, where X.X = 8.5 or 4.5.

Direct injection of aerosols or their precursors into the stratosphere is not considered explicitly as the stratospheric aerosol life cycle is not represented in the model. Instead, the radiative influence of stratospheric volcanic aerosols is accounted for by implementing vertically resolved spatial and temporal distributions of aerosol optical properties (monthly mean aerosol extinction, single-scattering albedo, and asymmetry factor) following *Stenchikov et al.* [1998]. This data set, originally developed for the Mount Pinatubo eruption based on satellite measurements by *Stenchikov et al.* [1998], has been extended to cover the historical time period (1850–1999) based on volcanic aerosol optical depths from *Sato et al.* [1993] and its updates [*Stenchikov et al.*, 2006]. Volcanic aerosol surface area density (SAD), used for calculating heterogeneous reaction rates, is derived from aerosol extinction centered at 1.0 μm following the relationship of *Thomason et al.* [1997].

We evaluate aerosol SAD implemented in the five-member ensemble of CM3 historical simulations [*John et al.*, 2012; *Austin et al.*, 2013] against size-resolved stratospheric aerosol concentrations provided by in situ measurements at Laramie (41°N, 105°W) from the University of Wyoming's optical particle counter (OPC) [*Deshler et al.*, 2003]. The OPC stratospheric aerosol measurements have recently been corrected for instrument calibration errors [*Kovilakam and Deshler*, 2015] and have been used to evaluate model-derived SADs [e.g., *Mills et al.*, 2016]. In Figures 1a and 1b, we reproduce the mean OPC SAD vertical profiles of *Kovilakam and Deshler* [2015] coincident with SADs derived from satellite extinction measurements from the Stratospheric Aerosol and Gas Experiment (SAGE) II and Halogen Occultation Experiment (HALOE), for volcanic (July 1991–December 1996) and nonvolcanic (1997–2005) time periods, and compare these to the mean aerosol SAD profile in the ensemble mean CM3 historical simulation. The CM3-calculated mean SAD profile above 15 km agrees very well with the OPC measurements after the Mount Pinatubo eruption (Figure 1a) but is an order of magnitude too low in the nonvolcanic period (Figure 1b). This implies that CM3 stratospheric ozone loss simulated in the period 1997–2005 with background aerosols is too low (see Figure S1 in the supporting information). Recent work shows that the algorithm of *Thomason et al.* [1997] (implemented in CM3) produces SADs comparable to OPC-derived SADs during the post-Pinatubo period but tends to underestimate OPC SADs during the nonvolcanic period when the aerosol size and loadings are too small [*Thomason et al.*, 2008; *SPARC*, 2006]. Future improvements to our model will implement these new methods to derive SADs during nonvolcanic periods such as the current period.

The CM3 historical simulations have been previously shown to generally reproduce well the observed total ozone column over the past several decades, except for a high bias in the tropics and southern midlatitudes [*Austin et al.*, 2013] (see also Figure S1). The positive bias in the southern midlatitudes is likely due to excessive transport of ozone by the Brewer-Dobson circulation from the tropics, where ozone is already high, to the midlatitudes [*Austin et al.*, 2013; *Eyring et al.*, 2013]. These deficiencies in the model will most likely have minor impact on our results as our analysis focuses on relative differences. Additionally, we evaluate the response of
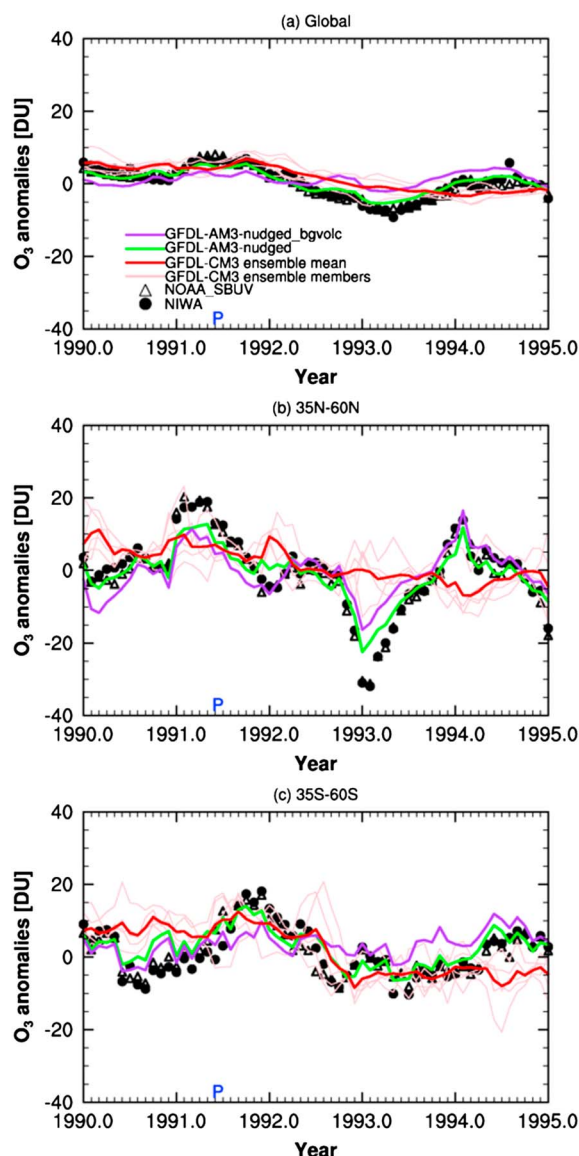
Figure 2. Total column ozone monthly mean anomalies (DU) from two observational data sets and model simulations for (a) global, (b) NH, and (c) SH midlatitudes. Anomalies were calculated relative to monthly mean total column ozone averaged over 1990–1999 period. Observed monthly average total ozone columns are taken from version 8.6 Solar Backscattered Ultra Violet (SBUV) data from the Nimbus-4 BUV, Nimbus-7 SBUV, and NOAA-9 through 18 SBUV/2 instruments [*Frith et al.*, 2013] (NOAA_SBUV) and version 2.8 of the monthly total column ozone from NIWA-BS total column ozone database [*Bodeker et al.*, 2005]. Blue P indicates the time of Pinatubo eruption.

ozone to volcanic aerosols by comparing monthly mean total ozone anomalies for the 5 year period encompassing the Mount Pinatubo eruption computed with CM3 historical simulations [*Austin et al.*, 2013] against observations [*Frith et al.*, 2013; *Bodeker et al.*, 2005] (Figure 2). The anomalies are calculated relative to the mean over 1990–1999 period; contributions due to quasi-biennial oscillation (QBO), El Niño–Southern Oscillation, solar cycle, and changing stratospheric chlorine and bromine have not been removed. Globally, the observations show a slow decline in monthly total column ozone after Mount Pinatubo eruption reaching a minimum of about −8 Dobson Units (DU) (1 DU = 0.001 atm cm) in early 1993. The ensemble mean is able to capture the observed variation in global monthly column ozone anomalies, although it is unable to reproduce the observed minimum (Figure 2a). One-ensemble member reproduces the observed global mean ozone minimum.

Despite depletion of stratospheric NO_2 in both hemispheres after the Pinatubo eruption [*Pawson et al.*, 2014, and references therein], observations indicate an interhemispheric asymmetry in the midlatitude ozone response to Pinatubo aerosols with enhanced ozone loss in the Northern Hemisphere (NH) midlatitudes and a small increase of ozone column in the Southern Hemisphere (SH) midlatitudes [*Randel et al.*, 1995]. Recent studies have attributed this asymmetry to enhanced ozone transport from the tropics to the SH extratropics that counterbalances the aerosol-induced ozone loss [*Poberaj et al.*, 2011; *Aquila et al.*, 2013; *Dhomse et al.*, 2015]. Observations show total column ozone decreases of up to 10 DU and 30 DU (relative to the

1990–1999 mean) in December 1991 and January 1993, respectively, in the NH midlatitudes (Figure 2b). In the SH midlatitudes, ozone column increases by 10 DU after the eruption, from July to December 1991, and then declines sharply reaching a minima of −10 DU in late 1992 (Figure 2c). The mean model does not reproduce variations in NH midlatitudes, although one-ensemble member is able to capture the column ozone decrease in December 1991 (Figure 2b). In the SH midlatitudes, the mean model is able to reproduce variability to some extent but has difficulty in capturing the timing of the increase in ozone column immediately after the eruption (Figure 2c).

Table 1. Overview of GFDL-CM3 Three-Member Ensemble Simulations Conducted to Assess the Influence of Elevated Volcanic Aerosols on Stratospheric Ozone Recovery

Experiment	Volcanic Aerosol Surface Area Density (SAD)	Greenhouse Gases (CO_2, CH_4, and N_2O) and Ozone Depleting Substances (ODSs)
RCP4.5_BG	1999	RCP4.5
RCP4.5_1860	1860	RCP4.5
RCP4.5_HM	Mean 1860–1999	RCP4.5
RCP8.5_BG	1999	RCP8.5
RCP8.5_1860	1860	RCP8.5
RCP8.5_HM	Mean 1860–1999	RCP8.5

Discrepancies in chemistry-climate model simulations of the interhemispheric asymmetry in the ozone response to Mount Pinatubo have been noted in previous studies [*Stratospheric Processes and their Role in Climate*, 2010, chapter 8]. Models forced with reanalyzed meteorological fields show better skill in simulating the enhanced ozone loss in the NH and the smaller ozone loss in the SH, pointing to the importance of dynamical forcing on ozone changes [e.g., *Shepherd et al.*, 2014; *Dhomse et al.*, 2015]. We performed two additional simulations of the atmospheric component of CM3 (AM3), with a similar model configuration as that used for the CM3 historical simulations, to shed light on the roles of dynamics and chemistry in the ozone response to volcanic forcing. Both of the simulations are nudged to NCEP-NCAR reanalysis zonal and meridional winds over the 1980–2010 period [*Lin et al.*, 2014; 2015] with the strength of nudging weakening with decreasing pressure (e.g., relaxing with a time scale of 6 h at the surface, 60 h by 100 hPa, and 600 h by 10 hPa). No nudging is implemented above 10 hPa. GFDL-AM3_nudged uses time-varying volcanic aerosols, while GFDL-AM3_nudged_bgvolc uses aerosol SAD values for 1999 from the volcanic aerosol data set described earlier. Ozone anomalies calculated for the GFDL-AM3_nudged simulation represent contributions from both dynamics and chemistry, while that for GFDL-AM3_nudged_bgvolc represents contributions only from dynamics.

As depicted by the green and purple lines in Figure 2, the GFDL-AM3_nudged and the GFDL-AM3_nudged_bgvolc show much better skill in reproducing the observed variations in the global mean column ozone anomalies and the interhemispheric asymmetry in the ozone response to Pinatubo aerosols compared to the historical ensemble mean. Ozone anomalies for GFDL-AM3_nudged_bgvolc are weaker than observed values, but the pattern is similar. Adding realistic volcanic forcing in GFDL-AM3_nudged brings the model simulation closer to observations suggesting that both chemistry and dynamics contribute to the ozone response to Pinatubo aerosols. Ozone anomalies from one ensemble-member of the free-running CM3 historical simulation match the observations suggesting that the free-running model may be able to simulate the chemical response; however, model internal dynamical variability overwhelms the chemical contribution resulting in biases in the historical ensemble mean. Alternatively, biases in the free-running simulations could also result from the misrepresentation of other real-world processes (e.g., dynamical and/or chemical responses from aerosols) that affect ozone. A large ensemble of free-running CM3 simulations would help to disentangle the purely chemical ozone response to volcanic aerosols from that driven by circulation changes whether resulting from internal variability or other forced dynamical response [e.g., *McGraw et al.*, 2016]. Absence of QBO could also explain why the model's dynamical response to forcing does not match the observations.

To address the goals of this study, we analyze results from three-member ensembles of transient CM3 simulations for the 2006–2100 time period, with concentrations of WMGGs, ODSs, and short-lived species emissions, following either the RCP4.5 [*Thomson et al.*, 2011] or RCP8.5 [*Riahi et al.*, 2011] climate forcing scenarios (Table 1). The simulated time evolution of effective equivalent stratospheric chlorine (calculated as $Cl + 60 \times Br_y$) at 63 hPa relative to 1980 for the scenarios considered here is shown in Figure S2. The ensemble members are initialized from the respective members of the CM3 historical simulation [*Austin et al.*, 2013]. For each climate forcing scenario, we consider three fixed levels of monthly-varying stratospheric aerosol loading repeated over the 95 years of each simulation. Three illustrative aerosol loadings are chosen arbitrarily from the time series implemented in the historical GFDL-CM3 simulations discussed earlier, and these are (1) extremely low volcanic aerosol loadings referred to as "background (BG)" set to year 1999 values, (2) low volcanic aerosol loadings set to 1860 values, and (3) moderate volcanic aerosol loadings set to historical mean (HM)

over the 1860–2000 period (Table 1). The simulations are denoted as RCPX.X_BG, RCPX.X_1860, and RCPX.X_HM, where X.X represents either 4.5 or 8.5. The "1860" is used nominally to represent low volcanic aerosols. The global annual mean volcanic aerosol optical depth (AOD) in the visible wavelength (550 nm) in RCPX.X_BG, RCPX.X_1860, and RCPX.X_HM simulations is 0.0005, 0.0045, and 0.013, respectively. Figure 1c shows the aerosol SAD vertical profiles at Laramie as implemented in the simulations. Our assumed background aerosol levels are too low compared with observations at Laramie during the nonvolcanic period of 1997–2005 (compare Figures 1b and 1c). The volcanic AOD in RCPX.X_1860 is close to that observed for tropical volcanic eruptions occurring in the 2000–2010 period, while that in RCPX.X_HM is similar to AOD observed for the moderate volcanic events in the mid-1980s [*Vernier et al.*, 2011].

For the analysis discussed below, we average results across ensemble members to better isolate the forced response to volcanic aerosols. Stratospheric ozone column is defined here as ozone concentrations integrated above 200 hPa. For each RCP scenario, we evaluate the impact of increased volcanic aerosols by comparing the results for 1860 and HM simulations against those of the corresponding BG simulation. Given that our BG aerosol SAD levels are lower than what has been observed for nonvolcanic periods, comparison of 1860 and HM results against BG will not be representative for recent years, over which we have observational constraints. The comparisons may, however, be illustrative for other conditions during the 21st century when background aerosols could fall lower than the year 1999 levels used here.

3. Impact of Volcanic Aerosols on Stratospheric Ozone

3.1. Ozone Column

We first analyze the long-term evolution of simulated global and regional stratospheric ozone column relative to 1980 levels in a manner consistent with previous multimodel projections [*Eyring et al.*, 2010b, 2013]. Figure 3 shows the 1980 baseline-adjusted time series of stratospheric ozone column from 1960 to 2100. Results are plotted for 1960–2005 from the CM3 historical simulations with time-varying stratospheric aerosols [*Austin et al.*, 2013] and for 2006–2100 from the RCPX.X_* simulations discussed above. Values are smoothed with a 1:2:1 filter applied 30 times iteratively ([see *Eyring et al.*, 2010b] smoothing was performed 50 times for polar region) to reduce interannual variability. In the 2006–2015 time frame, global annual mean stratospheric ozone column recovery in the RCPX.X_1860 simulations (blue lines) is similar to that in the RCPX.X_BG simulations (black lines), but it is slower in the RCPX.X_HM simulations (red lines; Figure 3a) with moderate volcanic aerosols. After the mid-2020s, the adjusted stratospheric ozone columns in both the RCPX.X_1860 and RCPX.X_HM simulations exceed the respective RCPX.X_BG simulations and recover to 1980 levels earlier than in the RCPX.X_BG simulations. Global stratospheric ozone column returns to 1980 levels in the RCP8.5_HM and RCP8.5_1860 simulations 3 to 7 years earlier (2045–2049) than in the RCP8.5_BG simulation (2052), while for the RCP4.5 scenario, return dates range from 2056 to 2071 compared to RCP4.5_BG in which ozone remains below 1980 levels throughout the 21st century. By 2100, the global stratospheric ozone column relative to 1980 levels is projected to range from 0.5 to 3 DU in the RCP4.5 and 11 to 13 DU in the RCP8.5 simulations with 1860 and HM aerosol loading, compared with −2.6 and 9.3 DU in the RCP4.5_BG and RCP8.5_BG simulations, respectively. The response of global mean stratospheric ozone column to elevated volcanic aerosols results from the combination of different responses in the tropics, midlatitudes, and polar regions as discussed below.

In the tropics, the annual mean stratospheric ozone column does not recover to 1980 levels (Figure 3b) in any of the simulations; however, it is greater in RCPX.X_1860 and RCPX.X_HM compared with the respective RCPX.X_BG simulations from about 2020 through the end of the 21st century. Previous multimodel studies [*Eyring et al.*, 2010a; *Eyring et al.*, 2013] attribute the nonrecovery of tropical stratospheric ozone column in simulations with increasing WMGGs and declining ODSs to a combination of (a) decreases in lower stratospheric ozone due to enhanced tropical upwelling from WMGG-induced warming and (b) increases in middle to upper stratospheric ozone from WMGG-induced cooling that slows down rates of chemical ozone destruction. Elevated volcanic aerosol loading in RCPX.X_1860 and RCPX.X_HM leads to warming of the tropical lower stratosphere relative to RCPX.X_BG (not shown) due to the absorption of longwave radiation, consistent with results of geoengineering model experiments in which stratospheric sulfate aerosols are artificially enhanced [*Tilmes et al.*, 2009; *Heckendorn et al.*, 2009; *Pitari et al.*, 2014]. This warming causes lower stratospheric ozone to decrease due to enhanced upwelling of ozone-poor air through the end of the 21st
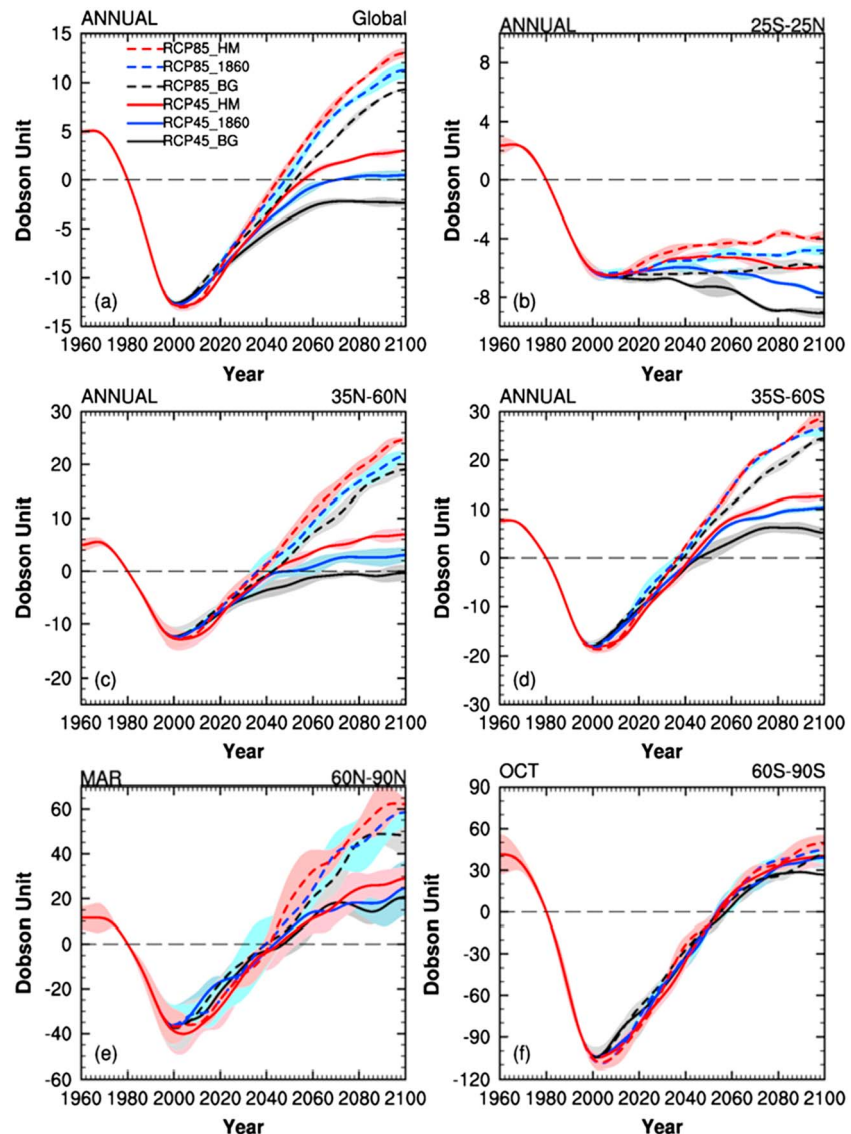
Figure 3. The 1980 baseline-adjusted time series of stratospheric ozone column (200–0 hPa) from 1960 to 2100 for the background (BG), 1860, and historical mean (HM) volcanic aerosols considered in RCP4.5 and RCP8.5 simulations. The panels show annual average (a) global mean, (b) in the tropics (25°N–25°S), (c) in the northern midlatitudes (35°N–60°N), (d) in the southern midlatitudes (35°S–60°S), and mean for March and October in the (e) Artic (60°N–90°N), and (f) Antarctic (60°S–90°S), respectively. Shaded areas indicate ±1 standard deviation across the three-ensemble members for each simulation. All values are smoothed with a 1:2:1 filter iteratively 30 times, except smoothing is applied 50 times over the polar regions.

century. In contrast, ozone concentrations increase in the middle to upper tropical stratosphere in RCPX. X_1860 and RCPX.X_HM relative to RCPX.X_BG due to the suppression of the NO_x-catalyzed ozone loss (discussed in the next section). Thus, the increased levels of stratospheric aerosols amplify both the WMGG-induced decrease of ozone in the lower stratosphere and the increase of ozone in the middle to upper stratosphere. The net effect of these opposing ozone responses is that at 2100 the annual mean tropical adjusted-stratospheric ozone column still decreases, but by less than in the corresponding RCPX. X_BG simulations, ranging from −7.9 to −6 DU in RCP4.5 and −4 to −5 DU in RCP8.5 simulations with 1860 and HM aerosol loading relative to 1980 values, in contrast with the −9.2 and −6.0 DU found in the RCP4.5_BG and RCP8.5_BG simulations, respectively.

In the midlatitudes, the RCPX.X_1860 and RCPX.X_HM projections of the adjusted-stratospheric ozone column (Figures 3c and 3d) evolve in a similar manner as that for the global mean. The ozone return dates

to 1980 values are significantly earlier in RCP4.5_1860 (2047) and RCP4.5_HM (2042) than in the RCP4.5_BG simulation in the NH midlatitudes but not in the SH midlatitudes. The ozone return dates are not statistically significantly different in the RCP8.5_1860 and RCP8.5_HM relative to RCP8.5_BG at either the northern or southern midlatitudes. At 2100, the annual mean adjusted-stratospheric ozone column in the northern midlatitudes is 0, 3, and 7 DU for RCP4.5 and 19, 22, and 25 DU for RCP8.5 with BG, 1860, and HM aerosol loadings, respectively. In the southern midlatitudes, the adjusted-stratospheric ozone column is 5, 10, and 12 DU for RCP4.5, and 24, 26, and 28 DU for RCP8.5 with BG, 1860, and HM aerosol loadings, respectively. Figure 3 also shows that the ozone column in the midlatitudes has greater sensitivity to the WMGG scenarios than in the tropics. This likely results from (a) stronger WMGG-induced stratospheric cooling that slows down ozone loss rates in the upper stratosphere leading to enhanced ozone [e.g., *Rosenfield et al.*, 2002; *Eyring et al.*, 2010a, 2010b, 2013], (b) a factor of 2.5 higher methane concentration in RCP8.5 [*Meinshausen et al.*, 2011] leading to greater ozone increase in lower stratosphere and troposphere [*Revell et al.*, 2012; *Young et al.*, 2013], and (c) greater WMGG-induced acceleration of Brewer-Dobson circulation resulting in increased stratosphere-troposphere exchange and ozone flux, particularly in the northern midlatitudes [*Bekki et al.*, 2011; *Pawson et al.*, 2014].

The long-term evolution of stratospheric ozone column relative to 1980 in the Arctic follows that of the global mean (Figures 3e). In March, the mean adjusted ozone loss for the 2006–2015 time period in the RCPX.X_1860 is similar to that in the RCPX.X_BG but is greater by 5 DU in both the RCP4.5_HM and RCP8.5_HM relative to the respective RCPX.X_BG simulations (Figure 3e). The ozone return dates are not statistically significantly different in the RCPX.X_1860 and RCPX.X_HM compared to that in the RCPX.X_BG. At 2100, the mean adjusted-stratospheric ozone column over Arctic in March is 21, 25, and 29 DU for RCP4.5, and 48, 58, and 62 DU for RCP8.5 with BG, 1860, and HM aerosol loadings, respectively. Figure 3e also shows that postrecovery, Arctic ozone column is sensitive to the RCP scenario as indicated by the ~40 DU difference between RCP4.5 and RCP8.5 at 2100 attributed to the stronger effect of transport-induced changes and chemical impacts in RCP8.5 consistent with previous studies [*Eyring et al.*, 2010b, 2013; *Dameris et al.*, 2014].

Over Antarctica in October, the evolution of adjusted-stratospheric ozone column is similar in the two RCP scenarios consistent with previous multimodel projections [*Eyring et al.*, 2013; *Dameris et al.*, 2014]; however, it is sensitive to elevated volcanic aerosols (Figure 3f), with greater aerosol concentrations suppressing ozone while halogen loading is still high, but enhancing ozone by year 2100. The mean adjusted ozone loss for the 2006–2015 time period is greater by 8 and 10 DU in the RCP4.5_1860 and RCP8.5_1860, respectively, and by 9 and 11 DU in the RCP4.5_HM and RCP8.5_HM, respectively, relative to the individual RCPX.X_BG simulations (Figure 3f). Similar to the Arctic, the ozone return dates are not sensitive to the aerosol loadings. At 2100, the adjusted ozone column is 28, 40, and 42 DU for RCP4.5, and 42, 45, and 50 DU for RCP8.5 with BG, 1860, and HM aerosol loadings, respectively.

3.2. Vertical Distribution of Zonal Mean Ozone Concentration

To decipher the trends in stratospheric ozone columns, we analyze the difference in the zonal mean ozone concentrations simulated for RCPX.X_1860 and RCPX.X_HM relative to the respective RCPX.X_BG simulations averaged over the 2006–2015 and 2091–2100 time periods. In the 2006–2015 period (Figure 4, top row) when stratospheric halogen loading is still sufficiently high, annual mean ozone concentrations are simulated to increase in the middle stratosphere and decrease in the lower stratosphere for RCPX.X_1860 and RCPX.X_HM relative to the respective RCPX.X_BG. These differences are weaker for the RCPX.X_1860 simulations with smaller volcanic aerosol loading than for the RCPX.X_HM simulations with greater aerosol loading. The zonal mean ozone differences are similar in the two RCPs, ranging from −0.1 to +0.2 ppmv in the RCP4.5_1860 and RCP8.5_1860 simulations, and −0.14 to +0.4 ppmv in the RCP4.5_HM and RCP8.5_HM simulations relative to the respective RCPX.X_BG. This similarity in ozone response to volcanic aerosols between the two RCPs is driven by the similarity in the WMGG and ODS projections in the early 21st century consistent with the findings of *Eyring et al.* [2013].

In the 2091–2100 time period (Figure 4, bottom row) when stratospheric halogen loading has diminished significantly (but is still above the natural background), stronger increases in annual mean ozone concentrations in the middle stratosphere and negligible decreases in the lower stratosphere are simulated for RCPX.X_1860 and RCPX.X_HM relative to the respective RCPX.X_BG. The importance of halogen chemistry has diminished over this time period as evidenced by the absence of statistically significant differences in ozone in the lower
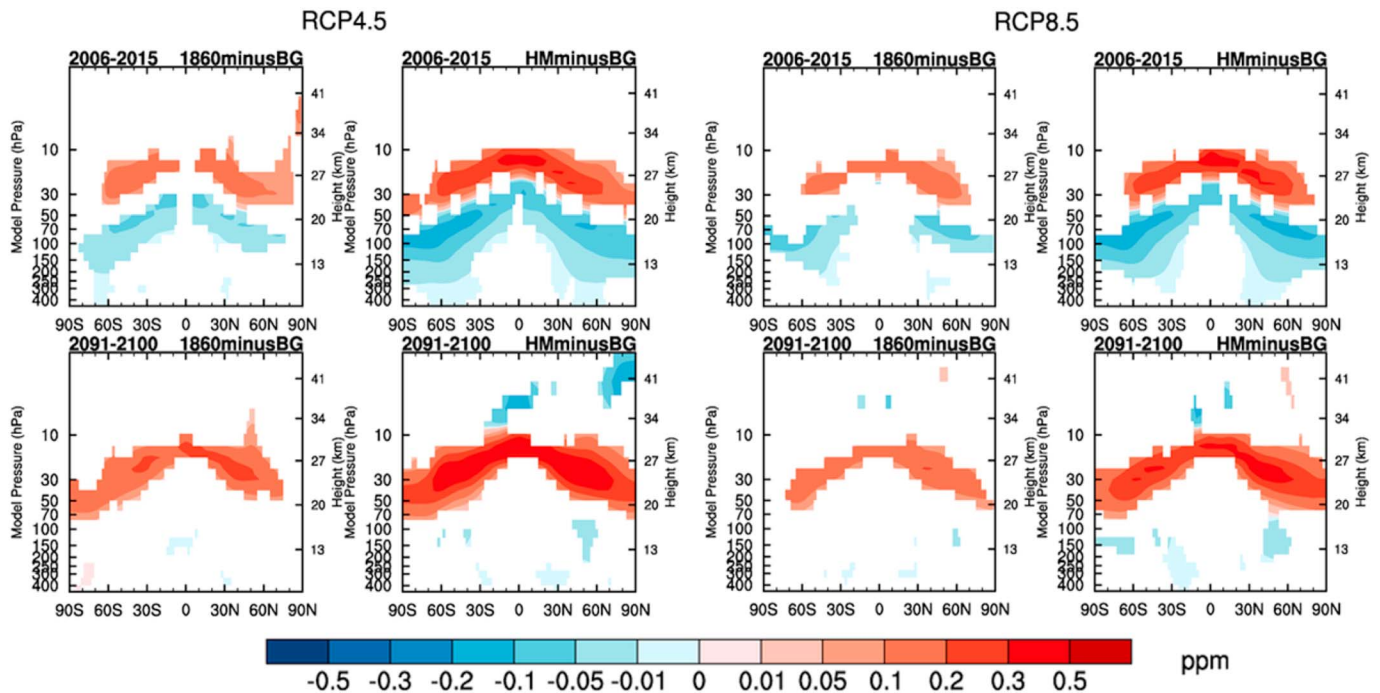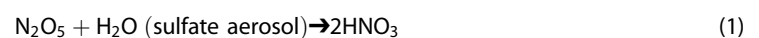
Figure 4. Difference in annual average zonal mean ozone concentration in (left two columns) RCP4.5 and (right two columns) RCP8.5 with 1860 and historical mean (HM) volcanic aerosols relative background (BG) volcanic conditions. Differences for mean (top row) 2006–2015 and (bottom row) 2091–2100 time periods. Only differences significant at 95% confidence level based on student's t test are shown.

stratosphere, where ozone decreased in response to volcanic aerosols for the 2006–2015 period (Figure 4). This is consistent with the results of *Austin et al.* [2013], who found a temporary increase in ozone column in response to volcanic eruptions in the prehalogen era. Like the 2006–2015 period, the ozone response to volcanic aerosols is stronger in the HM simulations with greater aerosol loading. The increase in ozone from increasing volcanic aerosol loadings at 2091–2100 is consistently weaker for RCP8.5 than that for RCP4.5, reflecting the role of greater methane loading in RCP8.5 which we discuss in the next section.

3.3. Chemical Partitioning Versus Aerosol Surface Area Density

Next, we analyze the mechanisms driving the stratospheric ozone response by examining the differences in chemical partitioning of reactive nitrogen (NO_y), reactive chlorine (Cl_y), and reactive bromine (Br_y), as a function of volcanic SADs, focusing on the northern midlatitudes. At 50°N, the simulated activated chlorine and bromine, represented as annual zonal mean ClO/Cl_y and BrO/Br_y ratios, increase with increasing aerosol SAD while activated NO_x (NO_x/NO_y) decreases in both RCP4.5 (Figures 5a–5e') and RCP8.5 (Figures 5f and 5j') scenarios; ClO/Cl_y and BrO/Br_y increase more strongly in the near term (2006–2015) when halogen loading is still high than in the future, particularly in the upper (17 hPa) stratosphere (Figures 5a, 5e, 5f, and 5j). Similar dependencies are simulated for the southern midlatitudes (not shown). Note that ClO/Cl_y values as high as 0.06 were observed close to local noon at northern midlatitudes on 22 March 1992 following the Mount Pinatubo eruption [*Fahey et al.*, 1993, Figure 4]. The annual zonal mean ClO/Cl_y values shown in Figures 5a' and 5f' are a factor of 4 too low compared to observations (Figure S3). Figure S3 shows the ClO/Cl_y at 70 hPa from our nudged model sampled close to local noon (35 < solar zenith angle <40) at midlatitudes on 17 September 1991 (representing background aerosol levels) and 22 March 1992 (with elevated aerosol levels due to the Mount Pinatubo eruption) when the observations were acquired [*Fahey et al.*, 1993]. The model does not reproduce the observed change in ClO/Cl_y with increasing aerosols well, which could indicate shortcomings in the model chemistry, or may reflect observational or sampling errors. The differences in the partitioning of NO_y and halogens are attributed to heterogeneous reactions occurring on stratospheric aerosol surfaces [see review of *Solomon*, 1999]. The key reaction linking volcanic aerosol changes to ozone depletion is the hydrolysis of N_2O_5 to nitric acid (HNO_3) that depletes NO_x:

$$N_2O_5 + H_2O \text{ (sulfate aerosol)} \rightarrow 2HNO_3 \qquad (1)$$
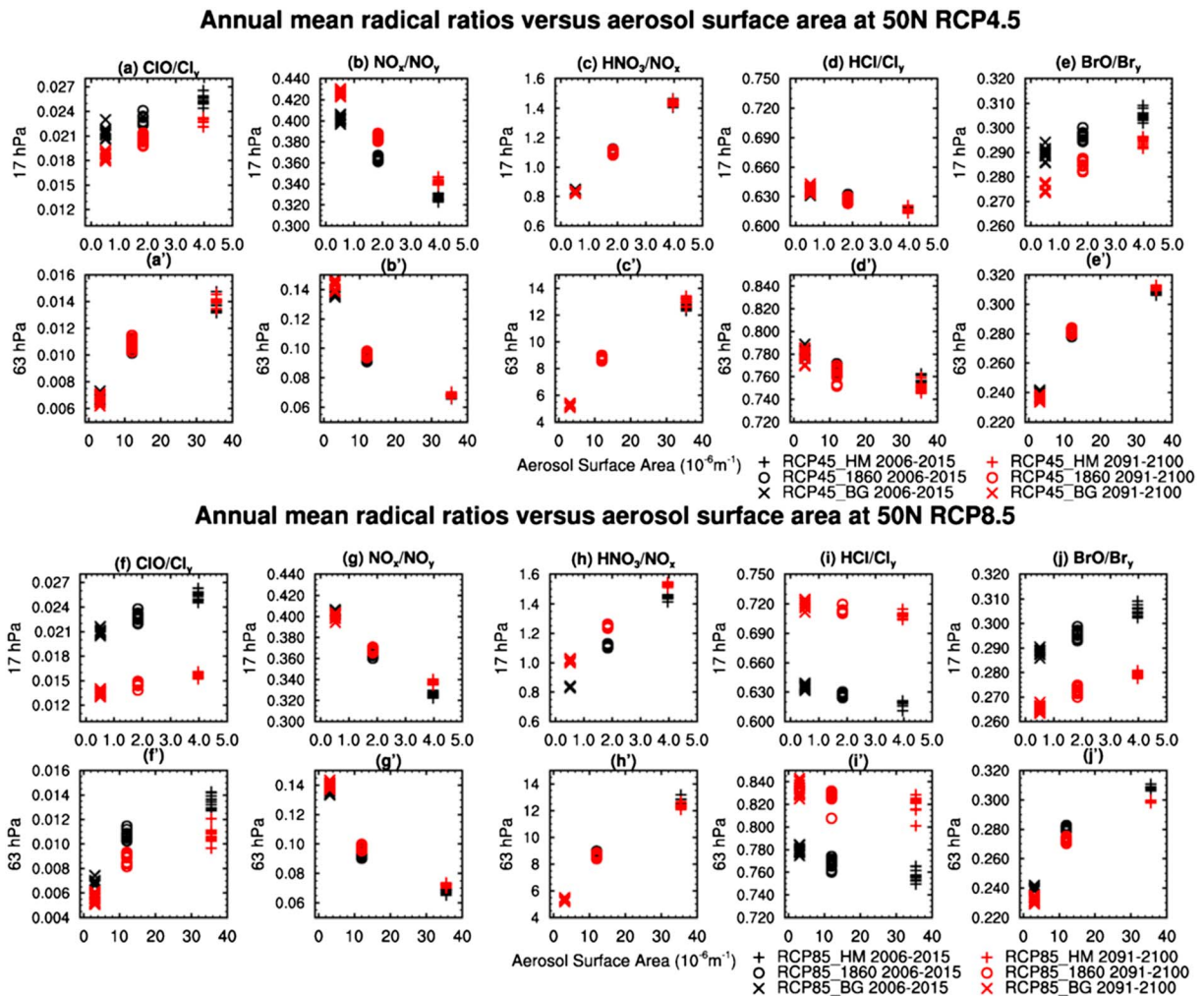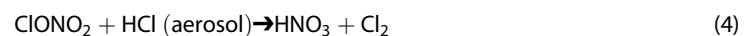
Figure 5. Annual zonal mean radical ratios as a function of volcanic aerosol surface area density (SAD) for 17 hPa and 63 hPa at 50°N. Values are individual years within 2006–2015 and 2091–2100 time periods averaged over three-ensemble members of the RCPX.X_BG, RCPX.X_1860 and RCPX.X_HM simulations, where X. X = (a–e and a′–e′) 4.5 and (f–j and f′–j′) 8.5.

Due to enhanced hydrolysis of N_2O_5 to HNO_3 as volcanic aerosol SAD increases, NO_x is depleted in RCPX. X_1860 and RCPX.X_HM relative to RCPX.X_BG resulting in lower NO_x/NO_y (Figures 5b, 5b′, 5g, and 5g′) and higher HNO_3/NO_x (Figures 5c, 5c′, 5h, and 5h′). This repartitioning causes NO_x-catalyzed ozone loss to be suppressed during both time periods. Since NO_x-induced ozone loss is dominant in the middle stratosphere [*Brasseur et al.*, 1999], this is where ozone is most enhanced in response to elevated volcanic aerosols (Figure 4).

Depleted NO_x not only reduces NO_x-catalyzed ozone loss but also perturbs halogen partitioning. Since less NO_2 is available to combine with ClO to produce the reservoir species, $ClONO_2$, more chlorine remains activated. Activated bromine is similarly increased by reduced formation of $BrONO_2$ although to a lesser extent. Thus, ClO/Cl_y and BrO/Br_y increase with increasing aerosol SADs, particularly in the 2006–2015 time frame with elevated halogen levels in the atmosphere (Figure 5). Additional heterogeneous reactions on sulfate aerosols also increase halogen activation:

$$ClONO_2 + H_2O \text{ (aerosol)} \rightarrow HOCl + HNO_3 \qquad (2)$$

$$BrONO_2 + H_2O \text{ (aerosol)} \rightarrow HNO_3 + HOBr \qquad (3)$$

$$ClONO_2 + HCl \text{ (aerosol)} \rightarrow HNO_3 + Cl_2 \qquad (4)$$

Typically, these occur on polar stratospheric clouds (solid NAT, water ice, and supercooled ternary solutions) in the extremely cold polar stratosphere; however, with enhanced aerosol surface areas, these reactions can proceed on liquid binary sulfate aerosols in the northern midlatitudes due to temperature and water vapor fluctuations [*Solomon*, 1999, and references therein]. The increase in halogen activation leads to enhanced ClO_x- and BrO_x-catalyzed ozone loss in the lower stratosphere where these catalytic cycles dominate.

Finally, gas-phase formation of HNO_3 via the reaction of $OH + NO_2 + M$ competes with reaction ((1)). As a result of this competition, higher aerosol SAD leads to OH increases (not shown) that enhance the HO_x-catalyzed ozone loss and increase the gas-phase conversion of hydrochloric acid (HCl) to reactive chlorine [*Granier and Brasseur*, 1992] via

$$HCl + OH \rightarrow Cl + H_2O \tag{5}$$

Reactions (4) and (5) lead to decreases in HCl as evident from decreasing HCl/Cl_y with increasing aerosol SAD in both the RCP4.5 (Figures 5d and 5d′) and RCP8.5 simulations (Figures 5i and 5i′).

For RCP4.5, the HNO_3/NO_x ratio is similar over the 2006–2015 and 2091–2100 time periods (Figures 5c and 5c′), but for RCP8.5 the HNO_3/NO_x ratio increases significantly between the two periods (Figures 5h and 5h′) due to the increased OH from the higher water vapor driven by a factor of 2.5 methane increase projected for RCP8.5 (as opposed to a small decrease for RCP4.5; see Figure 2). The increased OH in RCP8.5 increases the gas-phase production of HNO_3, thus making the chemistry less sensitive to aerosol SAD increases as evident from the gradual change in the NO_x/NO_y ratio with increasing SAD at 2091–2100 (Figures 5g and 5g′). This leads to a weaker ozone enhancement in RCP8.5 from elevated volcanic aerosols as compared to that in RCP4.5 at 2091–2100 (Figure 4).

The net effect on ozone of changes in Cl_y, Br_y, and NO_y partitioning in response to volcanic aerosols is thus a balance between competing effects on NO_x-, HO_x-, and halogen-catalyzed ozone loss cycles, with the net impact depending on the altitude, atmospheric halogen (and methane) loading, and volcanic aerosol loading. For the range of aerosol loadings considered here, the ozone response to volcanic aerosols does not saturate as suggested by *Prather* [1992].

4. Conclusions and Discussion

Analyses of transient three-member ensemble simulations of the GFDL-CM3 coupled chemistry-climate model following two future projection scenarios (RCP4.5 and RCP8.5) indicate that the response of stratospheric ozone to increases in volcanic aerosols varies systematically with altitude and halogen loading. In the early 21st century, increased halogen-catalyzed ozone loss in the lower stratosphere offsets suppressed NO_x-catalyzed ozone loss in the middle stratosphere, resulting in a largely similar recovery of global mean stratospheric ozone column in RCPX.X_1860 and RCPX.X_BG simulations; in the RCPX.X_HM simulations with greater volcanic aerosols, ozone column recovery is slower during this period due to the greater activation of halogen radicals causing increased ozone loss. After about the mid-2020s, when halogen levels have diminished (but are still above the natural background), the NO_x suppression by volcanic aerosols dominates, leading to stronger stratospheric ozone recovery in scenarios with elevated volcanic aerosols. Ozone column returns to 1980 levels in the mid-2040s in RCP8.5_1860 and RCP8.5_HM simulations (3 to 7 years earlier than in RCP8.5_BG), while its recovery date ranges from mid-2050s to early 2070s in the RCP4.5_1860 and RCP4.5_HM simulations compared with RCP4.5_BG in which it remains below 1980 levels through 2100. These results are sensitive to the amount of aerosol loading, as indicated by weaker responses in RCPX.X_1860 compared to those in RCPX.X_HM simulations. While the stratospheric ozone recovery by year 2100, relative to 1980, is greater in RCP8.5 than in RCP4.5 due to a factor of 2.5 greater methane in RCP8.5 compared to RCP4.5, the ozone increase from elevated volcanic aerosols relative to background is greater in RCP4.5 than in RCP8.5.

The long-term evolution of stratospheric ozone column in response to different future emissions scenarios varies by latitude regions [e.g., *Eyring et al.*, 2013]; elevated volcanic aerosols in the future act to enhance this variability. In the tropics, stratospheric ozone column does not respond to elevated aerosols until about 2020, but thereafter is enhanced by elevated volcanic aerosols in both RCP scenarios, although it remains below 1980 levels in all simulations. In the midlatitudes, stratospheric ozone column shows more sensitivity to

elevated volcanic aerosols in the NH than in the SH possibly because dynamical variability acts to enhance chemical ozone loss in the NH and decrease it in the SH [*Poberaj et al.*, 2011; *Aquila et al.*, 2013; *Dhomse et al.*, 2015]. This sensitivity is generally greater in RCP4.5 than in the RCP8.5 emission scenario. Over the polar regions, although the ozone return dates are insensitive to aerosol levels, the long-term evolution of stratospheric ozone column is sensitive to the amount of volcanic aerosol loading relative to the background. Arctic ozone columns in year 2100 are also sensitive to the greenhouse gas scenario.

Our findings are generally consistent with those of previous modeling studies that have analyzed the impact of volcanic aerosols [*Granier and Brasseur*, 1992; *Tie and Brasseur*, 1995; *Solomon et al.*, 1996; *Austin et al.*, 2013; *Aquila et al.*, 2013] and the impact of geoengineering via sulfate aerosols [*Heckendorn et al.*, 2009; *Tilmes et al.*, 2009; *Pitari et al.*, 2014] on stratospheric ozone in the presence of varying amounts of halogens. Our simulated ozone response in RCP4.5_HM can be directly compared with those simulated in multimodel geoengineering experiments conducted by imposing a constant sulfate aerosol surface area increase similar to that produced following the Mount Pinatubo eruption in the RCP4.5 reference scenario [*Pitari et al.*, 2014]. *Pitari et al.* find that increased aerosols would cause global ozone column to decrease in the 2040–2049 decade relative to the base RCP4.5 scenario but to increase after 2050, similar to our RCP4.5_HM results, although the timing of the ozone response is somewhat different. Our finding of increased polar stratospheric ozone loss in the presence of elevated volcanic aerosols for the 2006–2015 time period is consistent with the results of *Pitari et al.* who simulate a net reduction of 5% in polar ozone from elevated sulfate aerosols resulting from enhanced PSC formation. Our results are also consistent with the results of a more recent study in which an imposed factor of three enhancement in stratospheric sulfate over 2011 levels caused ozone loss to increase by up to 20 DU in the Antarctic and 15 DU in the Arctic [*Solomon et al.*, 2015].

As with any modeling study, our results are subject to errors resulting from model deficiencies. Model biases in stratospheric aerosol SAD and the ozone and atmospheric circulation response to these aerosols and other forcing agents (e.g., WMGGs, ODSs) will likely affect our results. For example, the better simulation of ozone response to the Mount Pinatubo aerosols in the nudged AM3 simulation compared to the free-running CM3 simulations demonstrates the influence of biases in atmospheric circulation. Our assumed background stratospheric aerosol SADs are much lower than those observed at Laramie during the nonvolcanic period of 1997–2005, which implies that our results are not representative for these years, but may be illustrative for other conditions during the coming century when background aerosols may fall lower than year 1999 levels. The stratospheric halogen source is treated in a simplified manner in our model to reduce computational cost; simulated Cl_y and Br_y have been shown to generally agree with existing observations but have some discrepancies, particularly in the tropics [*Austin and Wilson*, 2010], which may affect our results. CM3 does not explicitly simulate the emission of stratospheric aerosol precursors, aerosol formation, transport, growth, and loss processes after volcanic eruptions—processes that determine the aerosol SAD distribution and therefore affect the rate of heterogeneous reactions. Similar experiments with other global models that include these processes [e.g., *Mills et al.*, 2016] will help provide more robust estimates of the influence of stratospheric volcanic aerosols on ozone recovery [*Solomon et al.*, 2016].

Further, our results are specific to the idealized experiments conducted here, with imposed fixed levels of volcanic aerosols through the 21st century. In reality, stratospheric volcanic aerosol loadings will fluctuate, causing the timing and extent of ozone recovery to vary correspondingly. It would be worth exploring the influence of variable volcanic eruptions in the 21st century on the long-term evolution of stratospheric ozone. Finally, idealized volcanic-perturbation experiments conducted with multiple chemistry-climate models in support of Model Intercomparison Project on the climatic response to Volcanic forcing (VolMIP) [*Zanchettin et al.*, 2016] can help assess the robustness of the simulated stratospheric ozone response to strong volcanic forcings and can help identify the causes of differences in these responses.

Uncertainties in ozone projections and expected recovery dates have been recognized to come from uncertainties in assumed ODS and WMGG emission scenarios, interannual variability of ozone column, and diversity in model projections [*Eyring et al.*, 2013]. We show here that volcanic aerosol perturbations also contribute to this uncertainty, thus providing a knowledge base to interpret ozone results from future multimodel projections (such as ScenarioMIP) with volcanic forcing prescribed to be equal to a constant historical mean value [*O'Neill et al.*, 2016]. The novelty of our study lies in the use of transient simulations to 2100 using a state-of-the-art chemistry-climate model to demonstrate that the influence of volcanic aerosols on the

extent and timing of the ozone recovery varies with (a) greenhouse gas scenarios and (b) halogen loading. We have also highlighted the need to explore further the influence of increased methane concentrations on stratospheric ozone column under conditions of elevated stratospheric aerosols.

Predicting the timing and magnitude of volcanic eruptions on a global scale several decades into the future is currently impossible. Model simulations that consider hypothetical volcanic aerosol distributions based on recent measurements could help provide a lower limit of the influence of volcanic aerosols on stratospheric ozone. The response of stratospheric ozone to observed SAD over the 2000–2014 period for which we now have observational constraints [*Kremser et al.*, 2016, and references therein; *Solomon et al.*, 2016] can help provide estimates of the net effect of recent observed SAD on stratospheric ozone.

References

Aquila, V., L. D. Oman, R. Stolarski, A. R. Douglass, and P. A. Newman (2013), The response of ozone and nitrogen dioxide to the eruption of Mt. Pinatubo at southern and northern midlatitudes, *J. Atmos. Sci.*, *70*, 894–900, doi:10.1175/JAS-D-12-0143.1.

Austin, J., and R. J. Wilson (2010), Sensitivity of polar ozone to sea surface temperatures and halogen amounts, *J. Geophys. Res.*, *115*, D18303, doi:10.1029/2009JD013292.

Austin, J., L. W. Horowitz, M. D. Schwarzkopf, R. J. Wilson, and H. Levy II (2013), Stratospheric ozone and temperature simulated from the preindustrial era to the present day, *J. Clim.*, *26*, 3528–3543, doi:10.1175/JCLI-D-12-00162.1.

Baldwin, M. P., et al. (2001), The quasi-biennial oscillation, *Rev. Geophys.*, *39*, 179–229.

Barnes, E. A., A. M. Fiore, and L. W. Horowitz (2016), Detection of trends in surface ozone in the presence of climate variability, *J. Geophys. Res. Atmos.*, *121*, 6112–6129, doi:10.1002/2015JD024397.

Bekki, et al. (2011), Future ozone and its impact on surface UV, in *Scientific Assessment of Ozone Depletion: 2010*, in *Global Ozone Research and Monitoring Project—Report No. 52*, chap. 3, 516 pp., World Meteorol. Organ., Geneva, Switzerland.

Bodeker, G. E., H. Shiona, and H. Eskes (2005), Indicators of Antarctic ozone depletion, *Atmos. Chem. Phys.*, *5*, 2603–2615, doi:10.5194/ acp-5-2603-2005.

Brasseur, G. P., et al. (Eds.) (1999), *Atmospheric Chemistry and Global Change*, Oxford Univ. Press Inc., New York.

Collins, M., et al. (2013), Long-term climate change: Projections, commitments and irreversibility, in *Climate Change 2013: The Physical Science Basis. Contribution of Working Group I to the Fifth Assessment Report of the Intergovernmental Panel on Climate Change*, edited by T. F. Stocker et al., 1535 pp., Cambridge Univ. Press, Cambridge, U. K., and New York.

Dameris, M., et al. (2014), Update on polar ozone: Past, present, and future, chapter 3 in *Scientific Assessment of Ozone Depletion: 2014*, in *Global Ozone Research and Monitoring Project—Report No. 55*, 416pp, World Meteorol. Organ., Geneva, Switzerland.

Deshler, T., M. E. Hervig, D. J. Hofmann, J. M. Rosen, and J. B. Liley (2003), Thirty years of in situ stratospheric aerosol size distribution measurements from Laramie, Wyoming (41°N), using balloon-borne instruments, *J. Geophys. Res.*, *108*(D5), 4167, doi:10.1029/ 2002JD002514.

Dhomse, S. S., M. P. Chipperfield, W. Feng, R. Hossaini, G. W. Mann, and M. L. Santee (2015), Revisiting the hemispheric asymmetry in midlatitude ozone changes following the Mount Pinatubo eruption: A 3-D model study, *Geophys. Res. Lett.*, *42*, 3038–3047, doi:10.1002/ 2015GL063052.

Donner, L. J., et al. (2011), The dynamical core, physical parameterizations, and basic simulation characteristics of the atmospheric component of AM3 of the GFDL global coupled model CM3, *J. Clim.*, *24*, 3484–3519.

Eyring, V., et al. (2010a), Multi-model assessment of stratospheric ozone return dates and ozone recovery in CCMVal-2 models, *Atmos. Chem. Phys.*, *10*, 9451–9472, doi:10.5194/acp-10-9451-2010.

Eyring, V., et al. (2010b), Sensitivity of 21st century stratospheric ozone to greenhouse gas scenarios, *Geophys. Res. Lett.*, *37*, L16807, doi:10.1029/2010GL044443.

Eyring, V., et al. (2013), Long-term ozone changes and associated climate impacts in CMIP5 simulations, *J. Geophys. Res. Atmos*, *118*, 5029–5060, doi:10.1002/jgrd.50316.

Fahey, D. W., et al. (1993), In situ measurements constraining the role of sulphate aerosols in mid-latitude ozone depletion, *Nature*, *363*, 509–514.

Frith, S. M., et al. (2013), Multi-satellite merged ozone (O_3) profile and total column monthly L3 global 5.0deg Lat zones, version 1, NASA Goddard Earth Science Data and Information Services Center (GES DISC), Greenbelt, Md.

Granier, C., and G. Brasseur (1992), Impact of heterogeneous chemistry on model predictions of ozone changes, *J. Geophys. Res.*, *97*, 18,015–18,033, doi:10.1029/92JD02021.

Heckendorn, P., D. Weisenstein, S. Fueglistaler, B. P. Luo, E. Rozanov, M. Schraner, L. W. Thomason, and T. Peter (2009), The impact of geoengineering aerosols on stratospheric temperature and ozone, *Environ. Res. Lett.*, *4*, doi:10.1088/1748-9326/4/4/045108.

John, J., A. M. Fiore, V. Naik, L. W. Horowitz, and J. Dunne (2012), Climate versus emission drivers of methane lifetime from 1860 to 2100, *Atmos. Chem. Phys.*, *12*, 12021–12036, doi:10.5194/acp-12-12021-2012.

Junge, E., C. W. Chagnon, and J. E. Manson (1961), A world-wide stratospheric aerosol layer, *Science*, *133*, 1478–1479, doi:10.1126/ science.133.3463.1478-a.

Koike, M., N. B. Jones, W. A. Matthews, P. V. Johnston, R. L. McKenzie, D. Kinnison, and J. Rodriguez (1994), Impact of Pinatubo aerosols on the partitioning between NO_2 and HNO_3, *Geophys. Res. Lett.*, *21*, 597–600.

Kovilakam, M., and T. Deshler (2015), On the accuracy of stratospheric aerosol extinction derived from in situ size distribution measurements and surface area density derived from remote SAGE II and HALOE extinction measurements, *J. Geophys. Res. Atmos.*, *120*, 8426–8447, doi:10.1002/2015JD023303.

Kremser, S., et al. (2016), Stratospheric aerosol—Observations, processes, and impact on climate, *Rev. Geophys.*, *54*, 278–335, doi:10.1002/ 2015RG000511.

Lary, D. J., M. P. Chipperfield, R. Toumi, and T. Lenton (1996), Heterogeneous atmospheric bromine chemistry, *J. Geophys. Res.*, *101*, 1489–1504.

Lin, M., L. W. Horowitz, S. J. Oltmans, A. M. Fiore, and S. Fan (2014), Tropospheric ozone trends at Mauna Loa Observatory tied to decadal climate variability, *Nat. Geosci.*, *7*, 136–143.

Lin, M., A. M. Fiore, L. W. Horowitz, A. O. Langford, S. J. Oltmans, D. Tarasick, and H. E. Rieder (2015), Climate variability modulates western US ozone air quality in spring via deep stratospheric intrusions, *Nat. Commun.*, *6*, 7105, doi:10.1038/ncomms8105.

McCormick, P. M., L. W. Thomason, and C. Trepte (1995), Atmospheric effects of the Mt. Pinatubo eruption, *Nature*, *373*, 399–404, doi:10.1038/373399a0.

McGraw, E., A. Barnes, and C. Deser (2016), Reconciling the observed and modeled Southern Hemisphere circulation response to volcanic eruptions, *Geophys. Res. Lett.*, *43*, 7259–7266, doi:10.1002/2016GL069835.

Meinshausen, M., et al. (2011), The RCP greenhouse gas concentrations and their extension from 1765 to 2300, *Clim. Chang.* (Special Issue), doi:10.1007/s10584-011-0156-z.

Mills, M. J., et al. (2016), Global volcanic aerosol properties derived from emissions, 1990-2014, using CESM1(WACCM), *J. Geophys. Res. Atmos.*, *121*, 2332–2348, doi:10.1002/2015JD024290.

Naik, V., L. W. Horowitz, A. M. Fiore, P. Ginoux, J. Mao, A. M. Aghedo, and H. Levy II (2013), Impact of preindustrial to present-day changes in short-lived pollutant emissions on atmospheric composition and climate forcing, *J. Geophys. Res. Atmos.*, *118*, 8086–8110, doi:10.1002/jgrd.50608.

O'Neill, B. C., et al. (2016), The Scenario Model Intercomparison Project (ScenarioMIP) for CMIP6, *Geosci. Model Dev. Discuss.*, doi:10.5194/gmd-2016-84 in review.

Pawson, S., et al. (2014), Update on global ozone: Past, present, and future, in *Scientific Assessment of Ozone Depletion: 2014, Global Ozone Research and Monitoring Project–Report No. 55*, chap. 2, World Meteorol. Organ, Geneva, Switzerland.

Pitari, G., V. Aquila, B. Kravitz, A. Robock, S. Watanabe, I. Cionni, N. De Luca, G. Di Genova, E. Mancini, and S. Tilmes (2014), Stratospheric ozone response to sulfate geoengineering: Results from the Geoengineering Model Intercomparison Project (GeoMIP), *J. Geophys. Res. Atmos.*, *119*, 2629–2653, doi:10.1002/2013JD020566.

Poberaj, C. S., J. Staehelin, and D. Brunner (2011), Missing stratospheric ozone decrease at Southern Hemisphere middle latitudes after Mt. Pinatubo: A dynamical perspective, *J. Atmos. Sci.*, doi:10.1175/JAS-D-10-05004.1.

Prather, M. (1992), Catastrophic loss of stratospheric ozone in dense volcanic clouds, *J. Geophys. Res.*, *97*, 10187–10191, doi:10.1029/92JD00845.

Randel, W. J., J. M. Russell III, J. W. Waters, and L. Froidevaux (1995), Ozone and temperature changes in the stratosphere following the eruption of Mount Pinatubo, *J. Geophys. Res.*, *100*(D8), 16,753–16,764, doi:10.1029/95JD01001.

Revell, L. E., G. E. Bodeker, P. E. Huck, B. E. Williamson, and E. Rozanov (2012), The sensitivity of stratospheric ozone changes through the 21st century to N$_2$O and CH$_4$, *Atmos. Chem. Phys.*, *12*, 11309–11317, doi:10.5194/acp-12-11309-2012.

Riahi, K., S. Rao, V. Krey, C. Cho, V. Chirkov, G. Fischer, G. Kindermann, N. Nakicenovic, and P. Rafaj (2011), RCP8.5—A scenario of comparatively high greenhouse gas emissions, *Clim. Change*, *109*, 33–57, doi:10.1007/s10584-011-0149-y.

Rosenfield, J., A. R. Douglass, and D. B. Considine (2002), The impact of increasing carbon dioxide on ozone recovery, *J. Geophys. Res.*, *107*(D6), 4049, doi:10.1029/2001JD000824.

Sato, M., J. E. Hansen, M. P. McCormick, and J. B. Pollack (1993), Stratospheric aerosol optical depths, 1850–1990, *J. Geophys. Res.*, *98*, 22,987–22,994.

Shepherd, T., D. A. Plummer, J. F. Scinocca, M. I. Hegglin, V. E. Fioletov, M. C. Reader, E. Remsberg, T. von Clarmann, and H. J. Wang (2014), Reconciliation of halogen-induced ozone loss with the total-column ozone record, *Nat. Geosci.*, *7*, 443–449, doi:10.1038/ngeo2155.

Solomon, S. (1999), Stratospheric ozone depletion: A review of concepts and history, *Rev. Geophys.*, *37*, 275–316, doi:10.1029/1999RG900008.

Solomon, S., R. W. Portmann, R. R. Garcia, L. W. Thomason, L. R. Poole, and M. P. McCormick (1996), The role of aerosol variations in anthropogenic ozone depletion at northern mid-latitudes, *J. Geophys. Res.*, *101*, 6713–6727, doi:10.1029/95JD03353.

Solomon, S., D. Kinnison, J. Bandoro, and R. Garcia (2015), Simulation of polar ozone depletion: An update, *J. Geophys. Res. Atmos.*, *120*, 7958–7974, doi:10.1002/2015JD023365.

Solomon, S., D. J. Ivy, D. Kinnison, M. J. Mills, R. R. Neely III, and A. Schmidt (2016), Emergence of healing in the Antarctic ozone layer, *Science*, doi:10.1126/science.aae0061.

Stratospheric Processes and their Role in Climate (SPARC) (2006), SPARC Assessment of Stratospheric Aerosol Properties (ASAP). L. Thomason and Th. Peter (Eds.), SPARC report no. 4, WCRP-124, WMO/TD - no. 1295, available at www.sparc-climate.org/publications/sparc-reports/

Stratospheric Processes and their Role in Climate (2010), SPARC CCMVal report on the evaluation of chemistry-climate models.

Stenchikov, G. L., I. Kirchner, A. Robock, H.-F. Graf, J. C. Antuna, R. G. Grainger, A. Lambert, and L. Thomason (1998), Radiative forcing from the 1991 Mount Pinatubo volcanic eruption, *J. Geophys. Res.*, *103*, 13,837–13,858, doi:10.1029/98JD00693.

Stenchikov, G., K. Hamilton, R. J. Stouffer, A. Robock, V. Ramaswamy, B. Santer, and H.-F. Graf (2006), Arctic oscillation response to volcanic eruptions in the IPCC AR4 climate models, *J. Geophys. Res.*, *111*, D07107, doi:10.1029/2005JD006286.

Tilmes, S., R. R. Garcia, D. E. Kinnison, A. Gettelman, and P. J. Rasch (2009), Impact of geoengineered aerosols on the troposphere and stratosphere, *J. Geophys. Res.*, *114*, D12305, doi:10.1029/2008JD011420.

Thomason, L. W., L. R. Poole, and T. Deshler (1997), A global climatology of stratospheric aerosol surface area density deduced from Stratospheric Aerosol and Gas Experiment II measurements: 1984–1994, *J. Geophys. Res.*, *102*, 8967–8976, doi:10.1029/96JD02962.

Thomason, L. W., S. P. Burton, B.-P. Luo, and T. Peter (2008), SAGE II measurements of stratospheric aerosol properties at non-volcanic levels, *Atmos. Chem. Phys.*, *8*, 983–995, doi:10.5194/acp-8-983-2008.

Thomson, A. M., et al. (2011), RCP4.5: A pathway for stabilization of radiative forcing by 2100, *Clim. Change*, *109*, 77–94, doi:10.1016/s10584-011-0151-4.

Tie, X. X., and G. P. Brasseur (1995), The response of stratospheric ozone to volcanic eruptions: Sensitivity to atmospheric chlorine loading, *Geophys. Res. Lett.*, *22*, 3035–3038, doi:10.1029/95GL03057.

Vernier, J.-P., et al. (2011), Major influence of tropical volcanic eruptions on the stratospheric aerosol layer during the last decade, *Geophys. Res. Lett.*, *38*, L12807, doi:10.1029/2011GL047563.

Wennberg, P. O., et al. (1994), Removal of stratospheric ozone by radicals: In situ measurements of OH, HO$_2$, NO, NO$_2$, ClO, and BrO, *Science*, *266*, 398–404.

Westervelt, D. M., L. W. Horowitz, V. Naik, and D. L. Mauzerall (2015), Radiative forcing and climate response to projected 21st century aerosol decreases, *Atmos. Chem. Phys.*, *15*, 12,681–12,703, doi:10.5194/acp-15-12681-2015.

Young, P. J., et al. (2013), Pre-industrial to end 21st century projections of tropospheric ozone from the Atmospheric Chemistry and Climate Model Intercomparison Project (ACCMIP), *Atmos. Chem. Phys.*, *13*, 2063–2090, doi:10.5194/acp-13-2063-2013.

Zanchettin, D., et al. (2016), The Model Intercomparison Project on the climatic response to Volcanic forcing (VolMIP): Experimental design and forcing input data for CMIP6, *Geosci. Model Dev.*, *9*, 2701–2719, doi:10.5194/gmd-9-2701-2016.